Efficiency, Speed, and Scaling of Passive Dynamic Bipedal Walking

Mariano Garcia
Theoretical & Applied Mechanics
Cornell University
Ithaca, NY 14853

Anindya Chatterjee
Engineering Science & Mechanics
Penn State University
University Park, PA

Andy Ruina
Theoretical & Applied Mechanics
Cornell University
Ithaca, NY 14853

Submitted to *Dynamics and Stability of Systems*

July 29, 1998

Abstract

This paper addresses some performance limits of the two-dimensional passive-dynamic walking machines discovered by Tad McGeer. Energetic *in*efficiency is measured by downhill ground-slope γ needed to sustain gait, with $\gamma = 0$ being perfectly efficient. Speed is measured by the Froude number. We present some necessary conditions on the walker mass distribution to achieve perfectly efficient (zero-slope capable) walking for both kneed and straight-legged models. Our numerical investigations indicate that, consistent with a previous semi-analytical study of a simpler model, such walkers have two distinct gaits at arbitrarily small ground-slopes, for which only the longer-step gait is sometimes stable. Energy dissipation can be dominated by a term proportional to $(\text{speed})^2$ from tangential foot velocity at heelstrike and from kneestrike, or a term proportional to $(\text{speed})^4$ from normal foot collisions at heelstrike, depending on the gait, ground-slope, and walker design. For all zero-slope capable straight-legged walkers, the long-step gaits have no tangential foot velocity at heelstrike and are hence especially fast at low power or low ground-slope. A period doubling route to chaos is also numerically demonstrated for a kneed walker.

1 Introduction

Since humans and some potentially-useful robot designs use legged walking motions, it is interesting to consider the limits of possible performance of bipedal walking machines.

One natural modeling approach would be to consider the optimal performance of powered and controlled machines. Because animal nerve systems are so capable, because the energetic cost of thinking is so low, and because minimizing food use is advantageous, an energy-based optimization approach is likely to capture much of how people move (for example, see Beckett and Chang (1973), Alexander (1980), and Alexander (1991)). Energetic efficiency is one obvious goal of both biological and artificial locomotion and transportation systems. Other possible optimization criteria for consideration in the description of animal motion include peak muscle force, minimum-jerk, minimum-stress, maximum speed, etc., as discussed by Collins (1995), Nelson (1983), and Hatze (1989). The results of such optimizations, like the results of animal evolution, will probably often show limited use of muscles in walking, as shown in EMG studies by Basmajian and Tuttle (1973). So, given the uncertainties and complexities of many-degree-of-freedom optimization studies and the likely prediction of small muscle-usage (see Yamaguchi and Zajac (1990) for example), there is hope for insight from simpler approaches.

Although some motor activity is needed for walking, perhaps it can be neglected in some analyses like engine power can be neglected for much of the study of airplane flight, as argued by McGeer (1990a). A simple energy source (gravity) could then be used as a proxy for the small but essential muscle use of humans (or motor use in efficient robots). It is hoped, as must be ultimately checked, that many results thus obtained will be insensitive to the choice of the energy source. However, the use of gravity as an energy source (as opposed to a simple motor approximation) eliminates some arbitrariness, and simplifies simulation and physical experimental verification.

In this paper, we address walking performance issues in the context of gravity-powered walking machines, also mentioning some other properties of these machines.

2 Passive Dynamic Walking Machines

Passive dynamic walking machines that walk on shallow ground-slopes were first designed, simulated and built by Tad McGeer, who was inspired by the "ballistic" double- and triple-pendulum leg models proposed by Mochon and McMahon (1980). The McGeer-like passive-dynamic walking machines consist of hinged rigid bodies that make collisional and rolling contact with a sloped, rigid ground surface.

The two-dimensional kneed walking machine we study here, essentially a copy of McGeer's design, is shown schematically in figure 1. It consists of a *swing leg* (not in contact with the ground) and a *stance leg* (touching the ground), connected by a frictionless hinge at the *hip*. Extra mass is generally added at the hip serving as a crude model of an upper body. Each leg is composed of a rigid thigh and shank. The stance knee is locked. For kneed walkers, the swing knee is a frictionless hinge with a knee-stop preventing hyperextension. The two legs are assumed identical. Straight-legged (kneeless) walkers may be viewed as obtained from kneed walkers by permanently locking the knees.

A strobe photo of one of our working kneed physical models is shown in figure 2. A simulated walking cycle, using parameters measured from this model, is shown schematically in figure 3. Step period and stride length data from the physical model matched our simulation results to within about 5% at this ground-slope.

Three remarkable features that make the McGeer-like models so intriguing for both robotics and the understanding of animal gait are these:

1. **Existence of Gait.** A mechanism that resembles human legs in overall layout has an uncontrolled periodic motion that is rather anthropomorphic. A look at video recordings of McGeer's kneed machines (or our imitations of them), at passive-dynamic kneed simulations, or a comparison of passive-dynamic stick-figure strobe shots with human data (lower part of figure 3) certainly hint at the role of passive-dynamics in human gait.

2. **Efficiency of Gait.** These machines can walk down shallow ground-slopes, indicating small energy cost for horizontal transport. McGeer numerically found walking motions for ground-slopes as low as about 0.005 radians and we will show here predictions for walking at arbitrarily small ground-slopes.

3. **Stability of Gait.** For certain parameter combinations, McGeer found *stable* limit cycle motions for both straight-legged and kneed walkers as Goswami et al. (1996) and Garcia et al. (1998) later repeated for some straight-legged walkers, and we repeat and extend here

for kneed and straight-legged walkers.

Recent or current work is in progress by Fowble and Kuo (1996), Adolfsson et al. (1998), Coleman and Ruina (1998), and Garcia (1998) to extend McGeer's work on three-dimensional models. All of the above work hints at the possible role of passive-dynamics in producing *and* stabilizing efficient uncontrolled motion. But even unstable limit cycle motions of mechanical systems can (in principle) be stabilized with minimal energetic cost, as has been demonstrated for a three-dimensional walking model by Fowble and Kuo (1996) and implied by McGeer (1993). Thus, although the stability feature of some passive-dynamic designs is intriguing and possibly useful, even unstable passive-dynamic motions could be relevant to animals or machines.

3 Preliminaries

3.1 McGeer's Recipe

Our numerical analysis follows the program of McGeer (1990a) in treating a step as a Poincaré map. This approach is particularly well suited to the analysis of gait and is not limited to passive models. The technique is also described in some detail by Garcia et al. (1998) and Coleman et al. (1997).

A kneed walking *step* starts just after a heelstrike and ends after the next heelstrike. We assume that the swing knee is initially free to flex, and so we say that the walker is in *three-link mode*. Starting with initial conditions right after heelstrike, we solve the differential equations of motion for the three-link mode until kneestrike is detected. Using the angular-momentum based velocity-jump conditions that describe the knee collision (assumed to be instantaneous and plastic), we obtain new initial conditions for the start of the straight-leg or *two-link mode* (like McGeer, we use suction cups with adjustable leaks to enforce the plastic knee collision in our physical kneed models). We then solve the equations of motion for this straight-leg phase (with the knee locked) until heelstrike is detected (straight-legged walkers are always in two-link mode, and have no kneestrike during their gait). At the instant of double-support (i.e., contact at both feet), heelstrike occurs, which is also assumed to be instantaneous and plastic. The assumption of a plastic collision seems reasonable for the physical model where no macroscopic bounce or slip is observed. At heelstrike, the legs exchange stance and swing roles. Using the angular-momentum based velocity-jump conditions that describe the foot collision and renaming variables to switch legs, we obtain the initial conditions for the next three-link mode.

Following McGeer, we assume in our simulations that during the heelstrike collision, there is no impulse on the old stance foot. We have not tested this modeling assumption with force plate measurements, but it is self-consistent and gives simulation results which correctly predict the behavior of our experimental models. The heelstrike collision causes the knee on the new swing leg to unlock and flex, and the next step begins. This yields one evaluation of the "stride function", McGeer's name for the nonlinear return map (or Poincaré map) which describes one step.

If the new initial conditions after one step are exactly the same as those of the previous step, we have found a period-one limit-cycle (also called a fixed point of the map, or a *gait cycle*). If gait cycles do exist, they might be stable, in which case they can be found by direct simulation of the system over several steps, provided the initial conditions chosen are in the basin of attraction (as in Goswami et al. (1997)). Whether or not the fixed points are stable, they can be found by root-finding algorithms applied to the return map, as in McGeer (1990a) (also explained by Garcia et al. (1998)). At the fixed point, the eigenvalues of the Jacobian determine stability (all eigenvalues inside the unit circle implies linearized stability), something that is of secondary interest in this paper.

Although the root-finding involved in finding a gait cycle involves the numerical solution of n equations in n unknowns (where n is the dimension of the return map) there is no *a priori* guarantee that any gait cycles will exist for a given passive dynamic walking machine (i.e., a given set of masses, lengths, etc.) on a given ground-slope γ. In practice, all searches with all designs have found either zero, one, or two anthropomorphic period-one solutions for given machine parameters and ground-slope. Other non-anthropomorphic solutions may exist where the leg swings forward and backward more than once or the swing leg makes full revolutions (as in Garcia et al. (1998) and Coleman (1998)) but we do not consider them here.

3.1.1 Aside On The Map Dimensions

In general, one expects the dimension of the Poincaré map to be one less than the order of the system. For general straight-legged walkers, the map of the 4th-order system (two angles and two rates) is generally three-dimensional. For the superficially 6th-order kneed walker (three angles and three rates in three-link mode), the map is also only *three-dimensional* because the kneed walker is like a straight-legged walker for part of the swing-phase (after kneestrike). Thus, of the four numerically-calculated eigenvalues of McGeer (1990b) $(-0.001, 0.073, 0.261 \pm 0.363i)$, the first is actually *exactly* zero.

3.2 Reality Checks

Our numerical simulations are based on the assumptions above and not a general purpose rigid-body simulation code. Thus, some of the periodic solutions we find might violate various physically-relevant inequality conditions as discussed in McGeer (1990b). For the purposes of this paper, we neglect those violations in order to have solutions to study over the parameter range of interest; but when building a physical model, these issues are of interest. In our simulations, we can rationalize this neglect for each item of concern as follows.

1. **Foot scuffing.** In simulations of straight legged walkers, the swing leg inevitably passes through or scuffs the ground near mid-swing. In physical realizations of straight legged walkers, McGeer overcame this scuffing either with electromechanically-retractable ankles or with tiles placed on the ground (spaced for alternate stance-leg landings). A student group at Cornell University (Lattanzio et al. (1992)) overcame this difficulty using a passive mechanism that slightly retracted the swing leg. Kneed walkers may, but do not necessarily, avoid this scuffing by sufficiently flexing the swing knee at mid stride. For 3-D walking mechanisms (e.g.,. Fallis (1888)) and possibly in part for humans, foot scuffing can be avoided by side to side rocking. An unpowered scuffing solution could be changed to a non-scuffing solution by adding a small amount of actuation or a passive mechanism to slightly retract alternating legs for clearance.

2. **Positive knee-locking of the stance leg.** In our physical model, a joint-stop prevents knee hyperextension, but nothing stops knee flex, except residual suction in the knee cups just after kneestrike. In our simulations we assume that the stance knee is locked until it leaves the ground. Naturally-arising torques at the knee prevent unlocking in some but not all solutions. The simulation shown in figure 3 has a slight stance-leg unlocking impulse at kneestrike which we ignore in our simulations. The corresponding physical model does not collapse, presumably because the naturally-arising torques just after kneestrike are enough

to re-engage the knee stop. But even if they might not be, intermittent locking of a rotating joint can be performed with (theoretically) zero energy cost.

3. **Positive stance contact force and no slip.** The simulations assume contact between the stance leg and the ground. There is no contact tension in our simulations since all motions are well below the speed range ($v \approx \sqrt{gL}$) where tension is required to keep the stance leg in contact with the ground. The ground reaction forces and impulses are generally well within the friction cone for the foot-ramp interaction (say $\mu = 0.8$).

4. **Unlocking of the new swing leg.** As a leg switches from stance to swing in the simulations, it is allowed to flex or extend at the knee. That this motion is not hyperextension needs to be checked. Some of our simulated gaits have a small amount of this hyperextension, especially at near-zero ground-slopes. Allowance of such hyperextension could be designed into a low-energy controller.

5. **Ground release of the new swing leg.** As a leg switches from stance to swing, it is released from the ground. We assume that it does not penetrate the ground, but ground penetration could also be avoided by a low-energy controller.

3.3 Measures Of Performance

The performance issues of interest here are energetic cost and speed.

3.3.1 Slope And Specific Cost Of Transport

Since moving sideways in a gravitational field is workless, a rational dimensionless measure of energetic efficiency is somewhat problematic for transport or locomotion on level ground. The most reasonable measure of efficiency

$$\frac{\text{(fundamental minimum energetic cost)}}{\text{(actual cost)}} \tag{1}$$

is zero for all but the most ideal machines, for which it is undefined (0/0). The common dimensionless measure of (in)efficiency for locomotion is, however, the "specific cost of transport" or "specific resistance"

$$\eta = \frac{\text{(mechanical energy cost for transport)}}{\text{(weight)} \times \text{(distance travelled)}} \tag{2}$$

where the energy cost is also the energy dissipated. For steady walking motions, this reduces to (McGeer (1993))

$$\eta = \frac{\text{(energy dissipated per step)}}{\text{(walker weight)} \times \text{(step length)}} \tag{3}$$

In the case of gravitationally-powered walking, the energy dissipated is (weight) $\times$ (height drop over one step). So the inefficiency measure is

$$\eta = \sin\gamma \qquad \text{or} \qquad \eta = \tan\gamma \tag{4}$$

depending on whether it is distance along the path or horizontal distance that is being rewarded.

Other possible measures of transport cost are equivalent to the ground-slope γ at which the gait takes place (at least for small cost of transport). For example, an almost identical measure of inefficiency is F/N where F is the propulsive force necessary to maintain a constant (average) velocity, and N is the force normal to the transport surface. This is the common measure of rolling resistance. For rolling downhill, this ratio reduces to $\tan\gamma$. The coefficient of friction μ can be defined as the work per unit (distance $\times$ weight) required to drag an object on level ground. The same object can slide steadily down a ramp if $\tan\gamma = \mu$.

Finally, borrowing from aeronautics, a measure of aircraft performance when powered by gravity is the best achievable glide ratio, $\tan\gamma$, which is also approximately the lift to drag ratio of the aircraft (as in Katz (1994)).

For downhill locomotion on small ground-slopes, we can equate all of these inefficiency measures to

$$\text{inefficiency} = \gamma \tag{5}$$

Perfect transport efficiency is achieved by passive walking with $\gamma = 0$.

3.3.2 Speed Performance

Energetic efficiency does not credit speed nor penalize slowness. In practice, speed is also important. However, speed at a high energetic cost is of limited value, excepting for critical tasks such as hunting and escaping. Intuitive measures of merit, such as minimizing power for a given speed or maximizing speed at a given power are *dimensional* and thus lead to improvement by scale changes alone. For example, at a given ground-slope, the speed of all the designs we consider can be increased by a factor of ten with no increase in power by increasing the height by a factor of 100 and decreasing the mass by a factor of ten. That is, speed scales with $\sqrt{gl}$ and power scales with $mg^{3/2}l^{1/2}$, where g is the acceleration due to gravity, and l is a characteristic dimension, say the length of the walker's leg.

A simple nondimensional measure of merit that rewards speed is the square root of the Froude number,

$$\frac{v}{\sqrt{gl}} \tag{6}$$

at a fixed ground-slope. This measure cannot be affected by simple scaling changes. It is the natural measure recovered by redimensionalizing our non-dimensional results.

3.4 Kinetic Energy Lost In A Plastic Collision Of A Mechanism

The scalings we discuss depend essentially on the energy loss in the perfectly plastic (no-slip, no-bounce) heelstrike collision. General treatments of rigid body collisions, as well as references to the literature, may be found in works by Brach (1991), Chatterjee (1997), Chatterjee and Ruina (1998), and Brogliato (1996). We summarize below some facts relevant to this paper.

At the instant prior to heelstrike, let the velocity of the incipient contact point on the foot be $\dot{x}$ down the slope and $\dot{y}$ normal to the slope as in figure 4. See also Chatterjee and Garcia (1998).

Under the presumably reasonable assumption that no impulse from the ground acts at the trailing foot, the kinetic energy lost in the collision is equal to the product

$$\frac{1}{2}\begin{bmatrix}\dot{x} & \dot{y}\end{bmatrix}\underbrace{\begin{bmatrix}M_{11} & M_{12}\\ M_{21} & M_{22}\end{bmatrix}}_{\mathbf{M}}\begin{bmatrix}\dot{x}\\ \dot{y}\end{bmatrix} \tag{7}$$

where $\mathbf{M}$ is a 2×2, symmetric, positive semi-definite matrix that depends on the mass distribution and geometry of the walker. $\mathbf{M}$ is also configuration dependent, i.e., it depends on θ^*_{st}. We define $\mathbf{M}(0)$ as $\mathbf{M}$ in the limit as $\theta^*_{st} \to 0$. For the discussion that follows, we need not discuss explicit (and complicated) representation of $\mathbf{M}$ in terms of the mass distribution and configuration of the linkage. The only exception is for a simple first-order approximation of $\mathbf{M}$ in subsection 6.3.2; more discussion is found in a companion paper by Chatterjee and Garcia (1998).

4 The Simplest Walking Model

An extreme simplification of a straight-legged walker is the "minimal biped" of Alexander (1995) (a hip-mass on massless legs), made deterministic by the addition of infinitesimal point-masses at the feet. This "simplest walker" was studied in some detail in Garcia et al. (1998) with both perturbation methods and numerical simulation. The key results of that study are summarized below.

The simplest point-foot model has two gaits (two fixed points) at arbitrarily small ground-slopes. Of these, the long-step gait is stable at sufficiently small ground-slopes ($\gamma < 0.015$), while the short-step gait is unstable at all ground-slopes. (In Garcia et al. (1998) these two gaits are called the "long-period" and "short-period" gaits, possibly incorrectly intimating that the long-period gait is generally slower than the short-period gait.) As $\gamma \to 0$, the long-step gait motion approaches a symmetric motion that has normal heelstrike collisions ($\dot{x} = 0$ in figure 4). The short-step solution does not have this symmetry and the (quasi-massless) foot has a collision with a non-zero tangential component at heelstrike.

For this walker, both gait cycles were found to have stance angle θ_{st} or step-length proportional to $\gamma^{1/3}$ at small ground-slopes (see curves D in figure 9), while the step periods tend to (different) nonzero constants as the step length goes to zero. This implies a walking power consumption proportional to the fourth power of speed (for low speeds), for *both* gaits:

$$\text{Power} \propto m v^4 g^{-1/2} l^{-3/2}, \tag{8}$$

where m is the walker mass, v is the average walking velocity, g is the gravitational constant, and l is the walker's leg length. Equation 8 makes the unintuitive prediction that cost of transport increases with decreasing gravity and leg length.

This scaling also follows from the energy balance between collision losses and used-up gravitational potential energy, rather like for the rimless wheel described by McGeer (1990a). For this special case, $\mathbf{M}(0)$ of equation 9 is singular, and the only energy dissipation term comes from the $\dot{y}$ or normal component of the foot velocity at heelstrike, for both gaits. As explained partially in Alexander (1980) and for this model in Garcia et al. (1998), the normal velocity is proportional to both stance angle and stance angle rate. Since for small motions, the period is approximately independent of amplitude and the speeds are proportional to amplitude, the kinetic energy lost is proportional to the fourth power of step amplitude. The gravitational power available is proportional to step amplitude and ground-slope. Thus, (step amplitude)^4 $\propto$ (step amplitude) $\times$ (slope), and so (step amplitude) $\propto$ (slope)$^{1/3}$.

Between ground-slopes of $\gamma \approx .015$ to $\gamma \approx .019$ a period-doubling route to chaos was observed. Aside from the period doubling route to chaos, no other non period-one gaits were sought or found. Recently, Howell and Baillieul (1998) discovered a stable period-three gait at a slope of $\gamma \approx 0.0125$ and subsequent period-doublings (period-six, period-twelve, etc.) for this model.

In the rest of this paper we describe, as based on or at least tested by numerical integrations, which of the features above extend to more general straight-legged and kneed walkers. In some cases the equations of motion were derived with the help of symbolic algebra (Maple®) and the simulations were run using MATLAB®. The numerical methods and error checks used are similar to those described in Garcia et al. (1998).

5 More Complex Walking Models

5.1 Straight-Legged Pointfoot Walker With Non-Negligible Foot Mass

Describing mass distribution for a general straight-legged walker requires specifying center of mass position and moment of inertia. The studies of Goswami et al. (1996) and Goswami et al. (1997) were limited to a subset where the center of mass was on the foot-to-hip line (zero fore-aft offset), which reduced the number of parameters by one. We now consider a subset of the walkers of Goswami (and co-workers) with two finite point-masses: one at the hip and one at the foot (like the Goswami walkers, this subset also has point-feet). This simplification further reduces the number of parameters by one.

For the particular cases we study, the foot mass is still substantially smaller than the hip mass, but not infinitesimally small; the swing-leg angular velocity does not contribute to the pre-collision angular momentum about the new contact point (point of foot-collision at heelstrike), and the return map is two-dimensional, as it is with the simplest walker. Despite this simplification, we still resort to numerics when studying this class of models.

5.1.1 Solution Families And Scaling Laws

For the cases we have tried of these walkers, there are still two solutions at arbitrarily small ground-slopes. Again, the two solutions are distinguished by the long-step solution having essentially normal heelstrike collisions and the short-step solution having heelstrike collisions with a significant tangential component (a feature also approximately observed in McGeer (1993) and McGeer (1992) for a more complex walker).

For the simplest walker, with negligible foot mass, the only kinetic energy lost is that of the hip. When the feet have finite mass, however, the foot masses also lose energy at heelstrike. If the striking foot hits the ground with no tangential velocity, the loss scales as step length to the fourth power, giving a step length proportional to $\gamma^{1/3}$. With non-negligible-foot-mass, a tangential velocity component at heelstrike can change the energy-loss scaling.

This is demonstrated in figure 5, which shows stance angle as a function of γ for two walkers as described above. For the long-step solution, the stance angle remains proportional to the cube-root of the ground-slope. Unlike the simplest walker, the stance angle for the short-step solution is linearly proportional to γ at very small ground-slopes, and proportional to $\gamma^{1/3}$ at somewhat larger slopes. There is some transition region where the short-step scaling changes between the $\gamma^{1/3}$ and the γ scaling. So for the long-step gait, which is stable, power $\propto$ (speed)^4, while for the unstable short-step gait, power $\propto$ (speed)^2 below the transition region and $\propto$ (speed)^4 above the transition region.

5.1.2 The Short-Step Transition Region

The ground-slope at the transition region is governed by the ratio of the foot mass to the hip mass. If the foot mass is ρ times the hip mass instead of being totally negligible, then we will show later by asymptotic arguments that the transition occurs near a ground-slope proportional to $\rho^{3/2}$. Step length $\propto \gamma^{1/3}$ at ground-slopes where $\gamma >> \rho^{3/2}$, and step length $\propto \gamma$ at smaller slopes where $\gamma << \rho^{3/2}$ (see subsection 6.3).

Figure 5 shows two such transitions. Walker E has a foot mass of 0.1 and a hip mass of 0.8 (any units) and so $\rho_E = 0.125$. Walker F has a foot mass of 0.05 and a hip mass of 0.9 so $\rho_F = 0.0556$. Using the above rule of thumb, we expect the transition ground-slope for walker E to be proportional to ${\rho_E}^{3/2} = 0.125^{3/2} \approx 0.044$ and that of walker F to be proportional to ${\rho_F}^{3/2} = 0.0556^{3/2} \approx 0.013$

(these values are marked in figure 5). The ratio of the two critical slopes is equal to the ratio of the intersection values of the extrapolated best-fit lines from each walker's linear-scaling regime with an arbitrary cube-root-scaling line, as shown in the figure.

5.2 Generic Kneed And Straight-Legged Models

What about walkers with more general mass-distribution, non-zero foot radii, and foot offsets? Figure 6 shows stance angle θ_{st} at gait cycles occurring at different ground-slopes γ for the kneed walker of figure 3. Stable solutions are denoted by the heavy line. The dashed curve shows stance angle versus ground-slope for the straight-legged version (the same walker but with the knees always locked, $\theta_{sh} \equiv \theta_{th}$). Some observations about the solutions in figure 6 are as follows:

1. For both kneed and straight-legged walkers there are ground-slope γ regimes where there are either zero, one, or two solutions. This agrees with the observations and calculations of McGeer (1990a) and McGeer (1990b).

2. For the parameters used here, none of the straight-legged solutions and only a section of the kneed solution-locus are stable.

3. Along the kneed curve, kneestrike occurs later and later in the step, until at one end of the curve (point 1), heelstrike and kneestrike occur simultaneously. The locus of solutions terminates here since we do not investigate motions where heelstrike precedes kneestrike. In the analogous region on the dashed curve for the straight-legged walker (point 2), the heelstrike collision becomes increasingly tangential in nature, until the solution disappears. In this area, solutions and numerics become very unstable; we believe that the solution terminates at a ground-slope of about $\gamma = 0.056$ based on numerical evidence not discussed here.

4. At the other end of the long-step curve, the gait cycles are approaching initial conditions which approach falling backwards, i.e.,. the walker has just enough initial kinetic energy for the stance leg to make it past the vertical position. The same thing occurs at the analogous point on the dashed curve for the straight-legged walker. In both cases, this is the slowest gait found for the walkers.

5. All of the straight-leg solutions and some of the kneed solutions allow the foot to scuff the ground during the gait cycle.

6. Each walker needs a minimum ground-slope to sustain gait (about 0.016 rad for the straight-leg walker and about 0.02 rad for the kneed walker). So, these walkers are not perfectly efficient by the efficiency measures discussed earlier.

6 Walking At Near-Zero Slopes

As seen in the previous section, generic McGeer-like walking machines will typically have no steady walking motions below some nonzero ground-slope; thus, they have some nonzero inefficiency. But we have already seen that the point-foot walker with or without negligible foot mass can be perfectly efficient. Here we investigate the possibility of more general straight-legged and kneed walkers capable of zero-slope walking.

6.1 Necessary Conditions On Mass Distribution For Near-Zero-Slope Walking

Necessary conditions on the mass distribution for near-zero-slope kneed walkers are as follows:

1. As demonstrated in a companion paper by Chatterjee and Garcia (1998), based on some reasonable assumptions, if walking motions do occur at very small ground-slopes, these motions will be very slow. For these motions, gravity forces will be much bigger than inertia forces. As a result, the walker must be close to static equilibrium at all times. In the limit of zero slope, the walker configuration must approach a static equilibrium, or standing solution. Thus the foot-normal at the near-zero-slope walking condition must be directed towards the body center of mass.

2. At the instant of double-support, or heelstrike, both legs are straight and simultaneously touch the ground. As the ground-slope (hence, step length) goes to zero, the spacing between the legs at this instant also goes to zero. In the limiting case, the foot contact point must be that point on the foot which is farthest from the hip. Thus the normal to the foot contact point must pass through the hip.

3. From (1) and (2) the line from the hip through the body center of mass must intersect the foot curve normally at the place that will be the nominal contact point at zero-slope walking. For circular feet this is equivalent to the collinearity of the center of mass of the whole body, the hip, and the foot center (see figure 7).

4. For the swing leg to be in static equilibrium in three-link mode and to have zero knee-locking torque, the center of mass of the shank must lie directly under the knee, in the straight-leg configuration (see figure 7).

The simplification of these ideas for straight-legged walkers is described by item (3) above. These necessary statics-based conditions on the mass distribution do not guarantee that near-zero-slope walking solutions exist. Although we do not know general sufficient conditions, it is our experience that designs which meet these conditions and whose total center of mass is close to the hip do have walking motions for arbitrarily small ground-slopes.

The machines investigated by Goswami et al. (1996) and Goswami et al. (1997) satisfy these necessary conditions, so will probably walk at arbitrarily small ground-slopes.

Walkers satisfying the necessary conditions above have an $\mathbf{M}(0)$ which is diagonal.

6.2 Tuning Mass-Distribution For Near Zero-Slope Walking

After adjusting the mass parameters (*tuning*) for the walkers of figures 3 and 6 to match the conditions for zero-slope walking (figure 7), we found that both of these *tuned* walkers do indeed have walking motions at near-zero-slopes. Also, each walker now has *two* walking motions or gait cycles at all ground-slopes of $\gamma < 0.04$. The long-step, long-period cycle is stable at small ground-slopes, while the short-step, short-period cycle is unstable.

Figure 8 compares the shapes of the solution families of the 0% tuned kneed walker of figure 6 to its 100% tuned cousin. A solution family is also shown after the 0% walker has been 25% tuned to show how the long-step and short-step solution get closer at high ground-slopes and eventually merge into one curve. As the 100% tuned walker is de-tuned, the graphs change shape in the following ways.

1. The cusp at the origin breaks and the two solutions separate. The long-step solution remains stable but shifts to the right and no longer extends to zero ground-slope. Also, an unstable

region appears at very low speeds.

2. The short-step solution also shifts to the right; the point on this curve where the solution terminates moves up along the curve to the point where heelstrike and kneestrike are simultaneous.

3. At higher ground-slopes, the two solutions get closer and eventually merge as the walker is de-tuned. This merge point has a sharp corner, and occurs at lower and lower ground-slopes as the walker is de-tuned further. This merging does not seem to occur in straight-legged walkers.

Figure 9 shows short-step and long-step gait solutions for the abovementioned tuned straight-leg (A) and kneed (C) walkers, the point-foot walker of Garcia et al. (1998) (D), which is tuned by definition, and two other tuned straight-leg models (B and E). The parameters for each of these tuned walkers are listed in table 1. We make the following observations on their behavior.

1. All of these walkers can walk at arbitrarily small ground-slopes.

2. The simplest walking model (D) is the only one with both gaits having a step length $\propto \gamma^{1/3}$.

3. At the smallest ground-slopes, the tuned straight-leg walkers with finite foot mass (A, B, and E) each have one gait solution with step length $\propto \gamma$ (the short-step gait) and one solution with step length $\propto \gamma^{1/3}$ (the long-step gait). At steeper ground-slopes ($\gamma > 0.01$), all the gait solutions have step length $\propto \gamma^{1/3}$ as seen most clearly in figure 9b.

4. The tuned kneed walking solutions (C) *seem* to follow a similar pattern to the straight-leg solutions in figure 9. However, the long-step lengths of the tuned kneed walker are not proportional to $\gamma^{1/3}$ at very small ground-slopes. (Note how the "$\times$" symbols trail off at the left of the plot as if they were migrating towards the linear $y = ax$ scaling.) In fact, further numerical results indicate that this solution slowly changes to a linear scaling at extremely small ground-slopes ($\gamma \approx 0.00015$). Strictly speaking then, for the kneed walker, both the long-step and short-step gaits have step lengths $\propto \gamma$, although the longer period gait changes its scaling at extremely small ground-slopes.

5. Although it is not shown in the plots, all of the tuned long-step gaits have a certain ground-slope below which the gait is stable (down to zero slope).

Our numerical results indicate that a step length proportional to $\gamma^{1/3}$ is the longest step possible (and hence the smallest power consumption possible) at very small ground-slopes (i.e., low walking speeds).

As compared to walkers which do not meet the criteria in figure 7 above, tuned walkers will have a longer step length at a given small ground-slope (assuming other parameters such as masses, inertias, and leg lengths are held constant). This is illustrated by comparing figures 9 and 6 from section 5.2. At any ground-slope where gaits exist for both tuned and un-tuned walkers, the tuned walkers have a larger stance angle, and hence a longer step. Because the step periods are approximately the same for similarly-scaled tuned and un-tuned walkers, tuned walkers will also be faster than non-tuned walkers at a given ground-slope.

6.3 Energy Calculations And Scaling For Near-Zero-Slope Walking

Here, we show that for general walking machines that walk at near-zero ground-slopes, the step length for small slope γ is asymptotically proportional to either $\gamma^{1/3}$ or to γ. Thus far in our numerical investigations, as seen from the numerical results in figure 9, we find that all solutions for zero-slope-capable straight leg walkers apparently obey one of these two scalings.

6.3.1 Derivation Of Scaling Rule For Straight-Legged Walkers

Consider a straight-legged walker, with curved feet, at the instant prior to heelstrike. At this instant, $\theta_{st} = \theta_{th}$ (ignore θ_{sh} in figure 1 for the straight-leg case). The matrix $\mathbf{M}$ referred to earlier (see equation 7) is actually a function of θ_{st}, but since θ_{st} is small we write

$$\mathbf{M}(\theta_{st}) = \mathbf{M}(0) + \mathcal{O}(\theta_{st}). \tag{9}$$

For the present discussion, we mention that for zero-slope-capable walkers, $\mathbf{M}(0)$ will be diagonal when expressed in the coordinate system implicit in figure 4 and equation 7. In particular, its element M_{11} will be equal to the total mass of the walker, while element M_{22} will be smaller (a function of mass distribution and walker geometry). Finally, for a straight-leg, point-foot walker with a small foot mass (as considered in subsection 5.1), M_{22} is approximately equal (asymptotic) to the foot mass.

Recall figure 4. Now we express $\dot{x}$ and $\dot{y}$ in terms of $\dot{\theta}_{st}$ and $\dot{\theta}_{th}$, at the heelstrike configuration but just before heelstrike ($\theta^*_{th} = -\theta^*_{st}$). We define the length l to be the distance between the hip and the foot center. We obtain:

$$\begin{aligned} \dot{x} &= R(\dot{\theta}_{st} - \dot{\theta}_{th}) + l\cos\theta^*_{st}(\dot{\theta}_{st} - \dot{\theta}_{th}), \\ \dot{y} &= -l\sin\theta^*_{st}(\dot{\theta}_{st} + \dot{\theta}_{th}). \end{aligned} \tag{10}$$

Assume that as $\gamma \to 0$, the gait cycle step length θ^*_{st} is asymptotically of $\mathcal{O}(\gamma^p)$ for some $p > 0$. During the walking step, the angular rates $\dot{\theta}_{st}$ and $\dot{\theta}_{th}$ must also be $\mathcal{O}(\gamma^p)$. Moreover, at the instant of heelstrike, one or both of these rates must also be of the same order of magnitude $\mathcal{O}(\gamma^p)$ (these claims are proved by contradiction in Chatterjee and Garcia (1998)). Note that one would expect, from eq. 10, that $\dot{x} = \mathcal{O}(\gamma^p)$, while $\dot{y} = \mathcal{O}(\gamma^{2p})$.

Typically, at heelstrike, $\dot{x} \neq 0$ in Eq. 10, i.e., $\dot{\theta}_{st} - \dot{\theta}_{th} \neq 0$. As a result, for small γ, we find that the energy dissipation per step is proportional to $\dot{x}^2$ (see Eq. 7), or $\mathcal{O}(\gamma^{2p})$. Since the potential energy available per step is $\mathcal{O}(\gamma^{p+1})$ (step length $\times$ slope), we find that energy balance requires that $2p = p + 1$, or $p = 1$, i.e., the step length is proportional to γ.

On the other hand, for some gaits of some walkers, it may happen that $\dot{x} = 0$ at heelstrike, or $\dot{\theta}_{st} - \dot{\theta}_{th} = 0$. In those cases, the energy dissipation per step is $\mathcal{O}(\dot{y}^2)$ or $\mathcal{O}(\gamma^{4p})$. As before, the potential energy available per step is $\mathcal{O}(\gamma^{p+1})$. Energy balance therefore requires $4p = p + 1$, or $p = 1/3$, i.e., the step length *can* be proportional to $\gamma^{1/3}$. The same result holds true if $\dot{x}$ is not exactly zero, but a higher-order quantity, such that $\dot{\theta}_{st} - \dot{\theta}_{th} = \mathcal{O}(\gamma^{2p})$, or smaller. Thus, it is seen that the only two possibilities for step lengths proportional to γ^p are $p = 1$ and $p = 1/3$.

6.3.2 Predicting The Short-Step Transition Slope

for Point-Foot Walkers. Short-step gaits for straight-legged walkers with non-negligible foot masses and point-feet will typically exhibit a transition region between the linear and cube-root scalings, as discussed in subsection 5.1.2. Here, we consider the effect of adding a small but non-negligible foot mass of ρ times the total mass (here assumed nondimensionalized to unity), to the simplest point-foot walker.

Assuming θ_{st} is small, the kinetic energy dissipated in the collision is simply ($\mathbf{M}(0)$ is now diag[1 ρ]; see discussion of $\mathbf{M}(0)$ above also)

$$\frac{1}{2}\left(\dot{y}^2 + \rho\dot{x}^2\right) .$$

Assuming a step length comparable to γ^p as before, we find that energy balance requires

$$\gamma^{p+1} = \mathcal{O}(\gamma^{4p} + \rho\gamma^{2p})\,,$$

or

$$\gamma^{3p-1} + \rho\gamma^{p-1} = \mathcal{O}(1)\,.$$

For ρ any nonzero positive constant, this expression implies $p = 1$ as γ becomes arbitrarily small (i.e., step length $\propto \gamma$ at very small ground-slopes). On the other hand, for sufficiently small but fixed γ, taking smaller and smaller ρ, the scaling eventually reverts to $p = 1/3$. The transition occurs when the two left hand side terms above are comparable, or $\rho = \mathcal{O}(\gamma^{2p})$, in which case clearly $p = 1/3$. Thus, the transition occurs when $\rho = \mathcal{O}(\gamma^{2/3})$, or $\gamma = \mathcal{O}(\rho^{3/2})$ (see subsection 5.1.2).

Note that some of the preceding arguments depend on the assumption that the matrix $\mathbf{M}(0)$ of Eq. 9 is strictly positive definite. Its eigenvalues have been implicitly assumed to have comparable magnitudes. If its eigenvalues have disparate but finite nonzero magnitudes, then the scaling rules mentioned above will still be asymptotically accurate, though possibly only at very small ground-slopes.

6.3.3 Extension Of Scaling Argument To Kneed Walkers

Kneed walkers dissipate kinetic energy in collisions at both heelstrike as well as at kneestrike. For heelstrike, the energy loss calculations described above still hold: the pre-collision velocities are determined from the straight-leg or 2-link configuration, but the matrix $\mathbf{M}$ of equation 7 has to be calculated for the walker in three-link mode since the new swing leg is not constrained at the knee.

For kneed walkers, if the step length is proportional to γ^p, then the collision losses at kneestrike as well as heelstrike are each proportional to either γ^{2p}, or γ^{4p}, or perhaps even higher order, as $\gamma \to 0$. Of these, the heelstrike losses are already known to be at least $\mathcal{O}(\gamma^{4p})$. Thus, the total losses per step are either $\mathcal{O}(\gamma^{2p})$ or $\mathcal{O}(\gamma^{4p})$, leading to $p = 1$ or $p = 1/3$, respectively. In our simulations zero-slope-capable kneed walkers also have one solution that nearly obeys the high-efficiency ($p = 1/3$) scaling over the range of ground-slopes depicted in the figures. At even smaller ground-slopes, the knee collision eventually dominates and $p = 1$ scaling is recovered.

7 Chaos In Tuned Kneed Walkers

As shown for the point-foot walker in Garcia et al. (1996) and Garcia et al. (1998), and the walkers of Thuilot et al. (1997) and Goswami et al. (1996), tuned kneed walkers can also exhibit period doubling and chaotic gait, as shown in figure 10.

At small enough ground-slopes, the period-one gaits cycles are stable. The period-one motion becomes unstable at a slope of about 0.084, but a stable period-*two* gait appears, followed by a stable period-four gait, and so on (see figure 10). The walker continues to have stable (although possibly chaotic and not period-one) solutions at ground-slopes of up to about 0.103. At higher slopes we could not find stable walking motions for this kneed walker. For reasons we do not understand, the period-doubling occurs at higher ground-slopes than for the point-foot walker in Garcia et al. (1998) where the first period-doubling occurs at $\gamma \approx 0.015$ and the chaotic gait is at about $\gamma = 0.019$.

The existence of chaotic motions suggests that the "stepping stone" problem addressed by McGeer (1993) with active torque control might have passive or nearly passive solutions (as also mentioned in Garcia et al. (1998).

8 Concluding Remarks

We have found necessary conditions for arbitrarily small-slope passive dynamic walking. Remarkably, all the designs of this type that we have numerically tested have one solution that is stable and which is highly efficient (has no tangential velocity component at heelstrike and obeys the scaling rule 8). For the simplest walker of Garcia et al. (1998), the non-tangential collisions come from a time-reversal symmetry in the long-step gaits at very small ground-slopes. We do not know why the more general zero-slope-capable walkers also seem to have these efficient solutions.

Since the details of bipedal locomotion are intimately related to the mechanics of freely-swinging limbs it seems possible that the efficiency of human and efficient robot legs is related to the efficiency of similar, passive-dynamic mechanisms. Since we have described clear mechanical criteria for efficient passive-dynamic walking machines, similar criteria may apply for efficient human and robotic legs. Might it be more than coincidence that human legs nearly satisfy the necessary zero-slope conditions we have described? It remains to be seen if any of the scalings we have found are obeyed by an optimized but actively-powered bipedal design.

A quantitatively inclined reader will have noticed that the slopes and specific-costs of transport in our calculations are below those directly applicable to animals and physical machines. At higher ground-slopes or costs of transport other terms become important but the ideal effects we have described may still largely describe the scalings in passive walking.

Our results also imply that small parameter adjustments (in particular, fore-aft movement of the thigh and shank centers-of-mass) can influence biped gait characteristics rather remarkably.

9 Acknowledgement

Some of this work was done while Mariano Garcia was supported by an NSF graduate fellowship. Thanks to John Camp, Mario Gomes, Lanise Baidas and many other undergraduates who participated in various parts of this research, to Mike Coleman for many informative discussions throughout, and to Harry Dankowicz for pointing out the knee unlocking torque in one of our solutions.

References

Adolfsson, J., Dankowicz, H., and Nordmark, A. (1998). 3-D stable gait in passive bipedal mechanisms. *Proceedings of the European Mechanics Colloquium on Biology and Technology of Walking.*

Alexander, R. M. (1980). Optimum walking techniques for quadrupeds and bipeds. *J. Zoology, London*, 192:97–117.

Alexander, R. M. (1991). Energy-saving mechanisms in walking and running. *J. Exp. Biol*, 160:55–69.

Alexander, R. M. (1995). Simple models of human motion. *Applied Mechanics Review*, 48:461–469.

Basmajian, J. V. and Tuttle, R. (1973). EMG of locomotion in gorilla and man. In *Control of Posture and Locomotion*, pages 599–609. Plenum Press, New York.

Beckett, R. and Chang, K. (1973). An evaluation of the kinematics of gait by minimum energy. *Journal of Biomechanics*, pages 147–159.

Brach, R. M. (1991). *Mechanical Impact Dynamics: Rigid Body Collisions*. John Wiley and Sons, New York.

Brogliato, B. (1996). *Nonsmooth Impact Mechanics: Models, Dynamics and Control*. Springer, London, UK.

Chatterjee, A. (1997). *Rigid Body Collisions: Some General Considerations, New Collision Laws, and Some Experimental Data*. PhD thesis, Cornell University.

Chatterjee, A. and Garcia, M. (1998). Passive dynamic walking: Small slope implies low speed. In preparation.

Chatterjee, A. and Ruina, A. (1998). A new algebraic collision law based on impulse space considerations. Conditionally accepted for *Journal Of Applied Mechanics*, under revision.

Coleman, M., Chatterjee, A., and Ruina, A. (1997). Motions of a rimless spoked wheel: A simple 3D system with impacts. *Dynamics and Stability of Systems*, 12(3):139–160.

Coleman, M. J. (1998). *A Stability Study of a Three-dimensional Passive-Dynamic Model of Human Gait*. PhD thesis, Cornell University, Ithaca, NY.

Coleman, M. J. and Ruina, A. (1998). An uncontrolled walking toy that cannot stand still. *Physical Review Letters*, 80(16):3658–3661.

Collins, J. J. (1995). The redundant nature of locomotor optimization laws. *Journal of Biomechanics*, 28:251–267.

Fallis, G. T. (1888). Walking toy ("improvement in walking toys"). U. S. Patent, No. 376,588.

Fowble, J. V. and Kuo, A. D. (1996). Stability and control of passive locomotion in 3D. *Proceedings of the Conference on Biomechanics and Neural Control of Movement*, pages 28–29.

Garcia, M. (1998). *Stability, Scaling and Chaos in Passive-Dynamic Gait Models*. PhD thesis, Cornell University, Ithaca, NY.

Garcia, M., Chatterjee, A., Ruina, A., and Coleman, M. (1998). The simplest walking model: Stability, complexity, and scaling. *ASME Journal of Biomechanical Engineering*, 120(2):281–288.

Garcia, M., Ruina, A., Coleman, M., and Chatterjee, A. (1996). Passive-dynamic models of human gait. *Proceedings of the Conference on Biomechanics and Neural Control of Movement*, pages 32–33.

Goswami, A., Espiau, B., and Keramane, A. (1997). Limit cycles in a passive compass gait biped and passivity-mimicking control laws. *Journal of Autonomous Robots.* In Press.

Goswami, A., Thuilot, B., and Espiau, B. (1996). Compass-like bipedal robot part I: Stability and bifurcation of passive gaits. *INRIA Research Report No. 2996.*

Hatze, H. (1989). Neuromuscular control systems modeling: A critical survey of recent developments. *IEEE Transactions on Automatic Control*, AC-25:375–385.

Howell, G. W. and Baillieul, J. (1998). Simple controllable walking mechanisms which exhibit bifurcations. To appear in *Proceedings of the 37th IEEE Conference on Decision and Control.*

Katz, A. (1994). *Subsonic Airplane Performance.* Society of Automotive Engineers, Warrendale, PA.

Lattanzio, H., Kuenzler, G., and Reading, M. (May 1992). Passive dynamic walking. Project Report, Human Power Lab. Cornell University.

McGeer, T. (1990a). Passive dynamic walking. *International Journal of Robotics Research*, 9:62–82.

McGeer, T. (1990b). Passive walking with knees. *Proceedings of the IEEE Conference on Robotics and Automation*, 2:1640–1645.

McGeer, T. (1992). Principles of walking and running. In *Advances in Comparative and Environmental Physiology, Vol. 11.* Springer-Verlag, Berlin.

McGeer, T. (1993). Dynamics and control of bipedal locomotion. *Journal of Theoretical Biology*, 163:277–314.

Mochon, S. and McMahon, T. (1980). Ballistic walking: An improved model. *Mathematical Biosciences*, 52:241–260.

Nelson, W. L. (1983). Physical principles for economies of skilled movements. *Biological Cybernetics*, 46:135–147.

Thuilot, B., Goswami, A., and Espiau, B. (1997). Bifurcation and chaos in a simple passive bipedal gait. *IEEE International Conference on Robotics and Automation*.

Winter, D. A. (1987). *The Biomechanics and Motor Control of Human Gait*. University of Waterloo Press.

Yamaguchi, G. T. and Zajac, F. E. (1990). Restoring unassisted natural gait to paraplegics via functional neuromuscular stimulation: A computer simulation study. *IEEE Transactions on Biomedical Engineering*, 37:886–902.

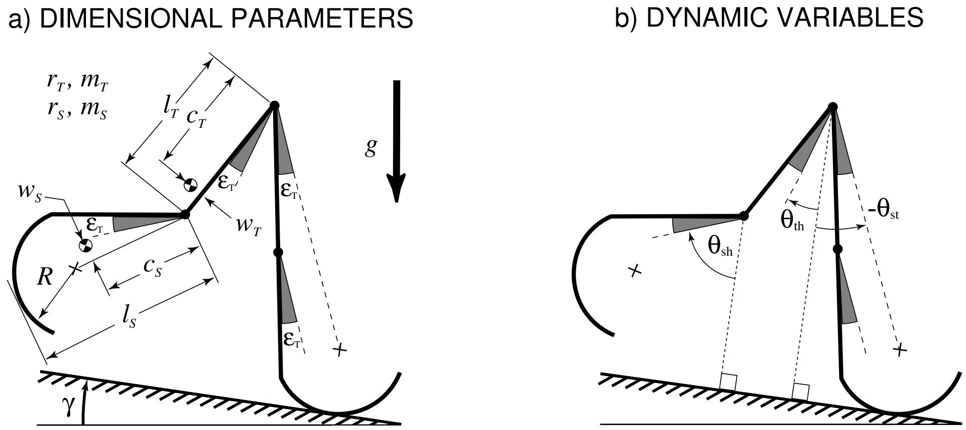

Figure 1: Our description of McGeer's kneed walking model. Shown above are (a) model parameters, and (b) dynamic variables. Radii of gyration and masses of thigh and shank are denoted by r_t, m_t, r_s, and m_s, respectively. The foot is a circular arc centered at the "+". ε_T is defined to be the angle between the stance thigh and the line connecting the hip to the foot center. Dynamic variable values θ_{st}, θ_{th}, and θ_{sh} are measured from ground-normal to lines offset by ε_T from their respective segments. A stop (not shown) at each knee prevents hyperextension of either knee. In straight-legged models, the knee is locked.

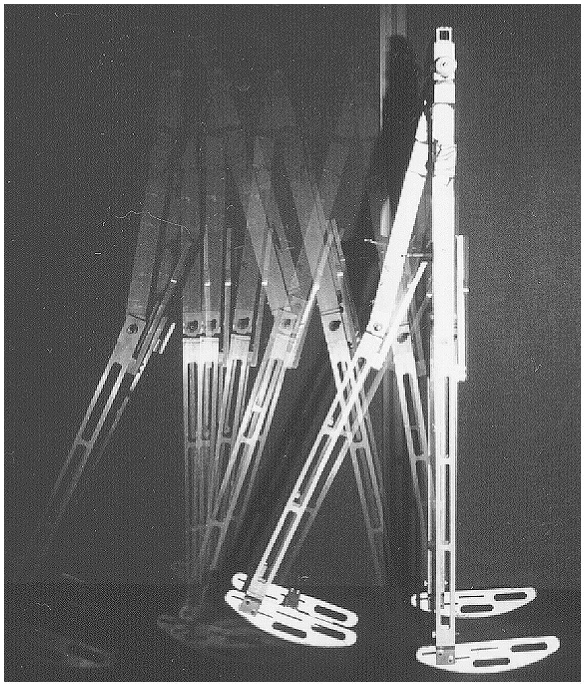

Figure 2: Strobe photo of our passive dynamic walker walking down a shallow ramp in our lab. The double leg-set constrains motions to a plane. The simulation we show in figure 3 uses the parameters measured from this walker. Photo by R. Pratap.

Walker	l_t	w_t	m_t	r_t	c_t	l_s	w_s	m_s	r_s	c_s	R	ε_T
A	0.35	-0.023	2.345	0.1882	0.084	0.46	0.022	1.013	0.1226	0.17	0.2	0.097
B	0.5	0	0.4	0	0	0.5	0	0.1	0	0.5	0.2	0
C	0.35	-0.023	2.345	0.1882	0.084	0.46	0.022	1.013	0.1226	0.17	0.2	0.097
D	0.5	0	∞	0	0	0.5	0	1	0	0.5	0	0
E	0.5	0	0.4	0	0	0.5	0	0.1	0	0.5	0	0

Table 1: Parameters for several tuned walkers in any consistent units. Only C has knees. Straight-legged walkers A, B, D, and E have redundant parameters since the shank and thigh are rigidly connected. m_t and m_s are the thigh and shank masses. For B, D, and E m_s is a point-mass at the bottom of the foot.

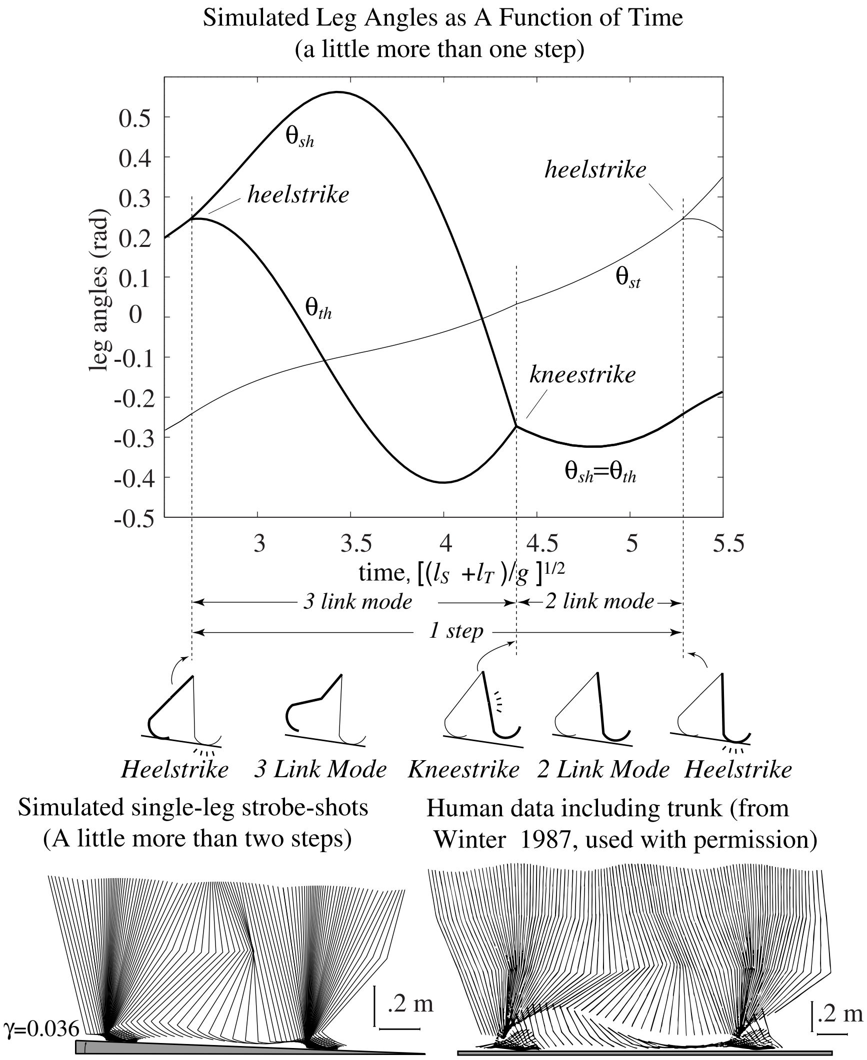

Figure 3: Simulated gait cycle (ours, similar to McGeer's). Angles of leg segments are shown from just before a heelstrike to just after the next heelstrike in a steady stable gait of the walker in figure 1. The heavy line on the graph corresponds to the motion of the heavy-line leg on the small cartoon under the graph. At the start of the step, this is the stance leg, but it becomes the swing leg just after the first heelstrike shown, and again becomes the stance leg after the second heelstrike shown. In general, the angular velocities of the joint segments have discontinuities at kneestrike and heelstrike, which would appear as kinks in the angle trajectories above. The kinks at kneestrike do not happen to be prominent in this particular simulation. The strobe-like picture of the walker simulation shows the anthropomorphic nature of the gait; it was created from the simulated gait cycle in the graph. Measured human data (including trunk, with a smaller scale and a longer stride) from Winter (1987) is shown to the right. The parameters used in the simulation are those of one of our working physical models; the dimensional parameters are as follows: $l_t = 0.35\text{m}$, $w_t = 0\text{m}$, $m_t = 2.345\text{kg}$, $r_t = 0.099\text{m}$, $c_t = 0.091\text{m}$, $l_s = 0.46\text{m}$, $w_s = 0.025\text{m}$, $m_s = 1.013\text{kg}$, $r_s = 0.197\text{m}$, $c_s = 0.17\text{m}$, $R = 0.2\text{m}$, $\gamma = 0.036\text{rad}, g = 9.81\text{m/s}^2, \varepsilon_T = 0.097\text{rad}$.

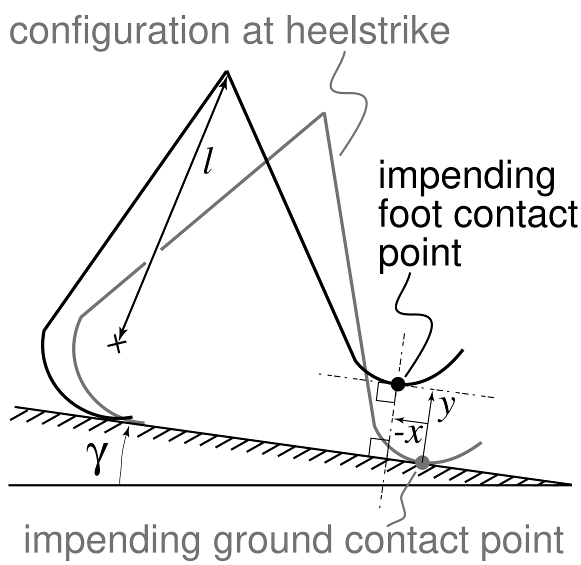

Figure 4: Close to heelstrike, the x and y coordinates of any point on the foot relative to any point on the ground can be used as generalized coordinates to describe the configuration of the walker. Since we are examining a known gait cycle, these points can be chosen to be the points at which contact will occur at heelstrike. l is the distance between the foot center and the hip.

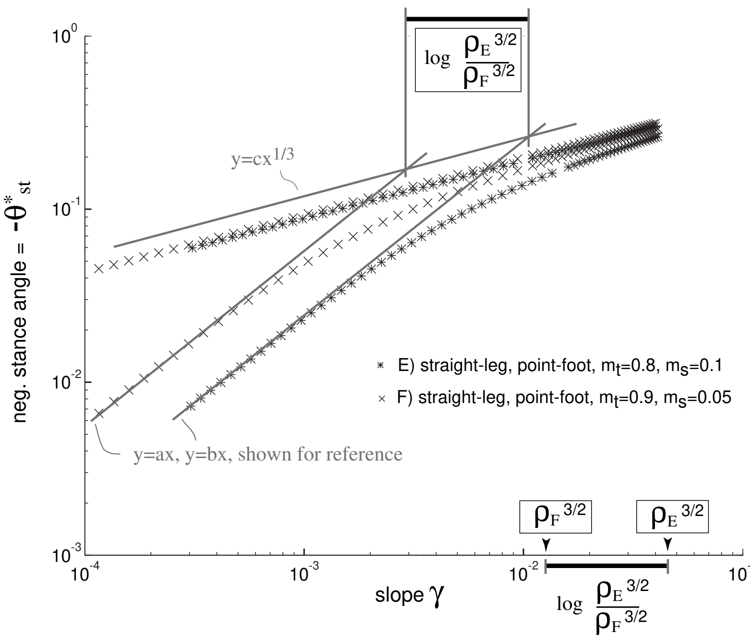

Figure 5: Scaling transition comparison for two point-foot walkers. Data for walker E is shown again in figures 9. Parameters for walker E are shown in table 1. Walker F has a foot mass of 0.05 and a hip mass of 0.9. At large ground-slopes ($\gamma \gg \rho^{3/2}$), the walker stance angles scale as $\gamma^{1/3}$. The predicted critical slopes for walkers E and F are shown at the bottom of the plot. Above these slopes, we expect the stance angle to be proportional to the cube root of the ground-slope. The ratio of the two critical slopes is nearly identical to the ratio of the intersections of the two best-fit lines in the linear scaling regimes with a cube-root scaling line. The solution curves for the “simplest” walker would show as parallel lines more or less on top of the upper curves in this figure. Note that the “×” symbol used here refers to data from a different walker than in figure 9.

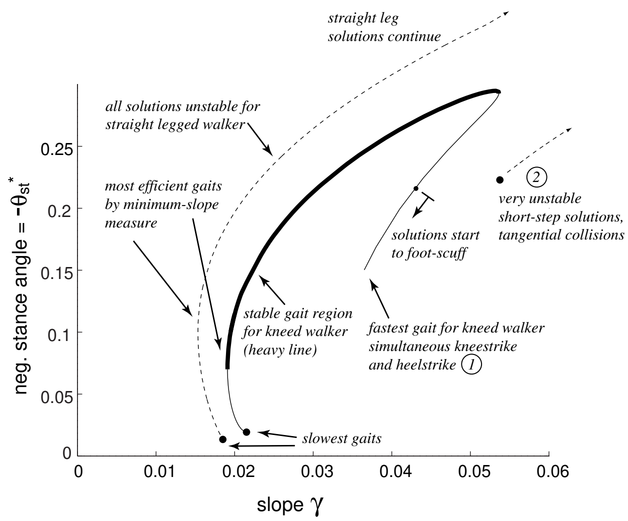

Figure 6: Numerically-calculated locus of solutions showing fixed points of stance angle as a function of ground-slope for our physical kneed walking model (solid line) and for the same model but with the knees locked (dashed line). The thick portion of the solid line denotes stable solutions for the kneed walker.

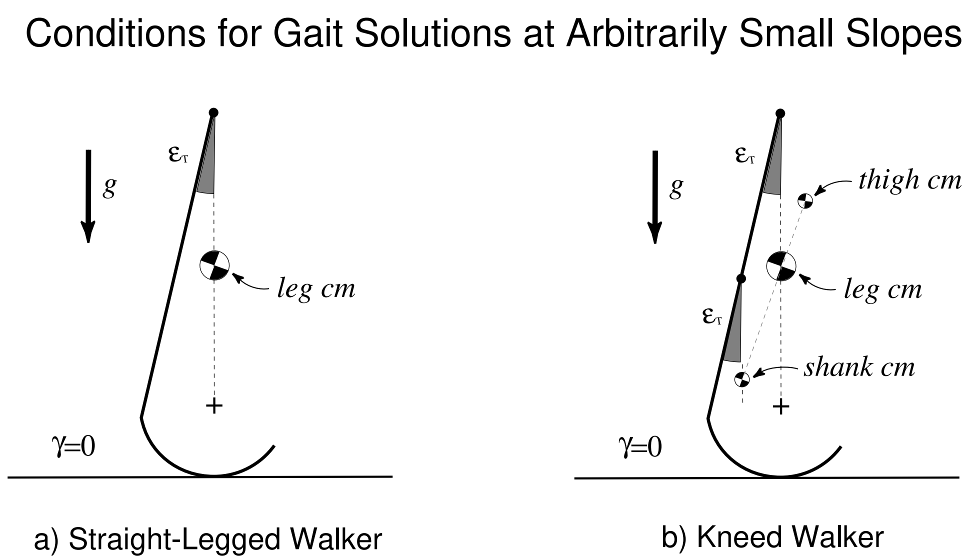

Figure 7: To walk at arbitrarily shallow ground-slopes, a walker must allow a static standing solution at zero slope with the stance leg locked, the swing leg unlocked, the legs parallel, and the hip directly above the foot contact. These conditions are shown graphically for (a) a straight leg, and (b) kneed walker.

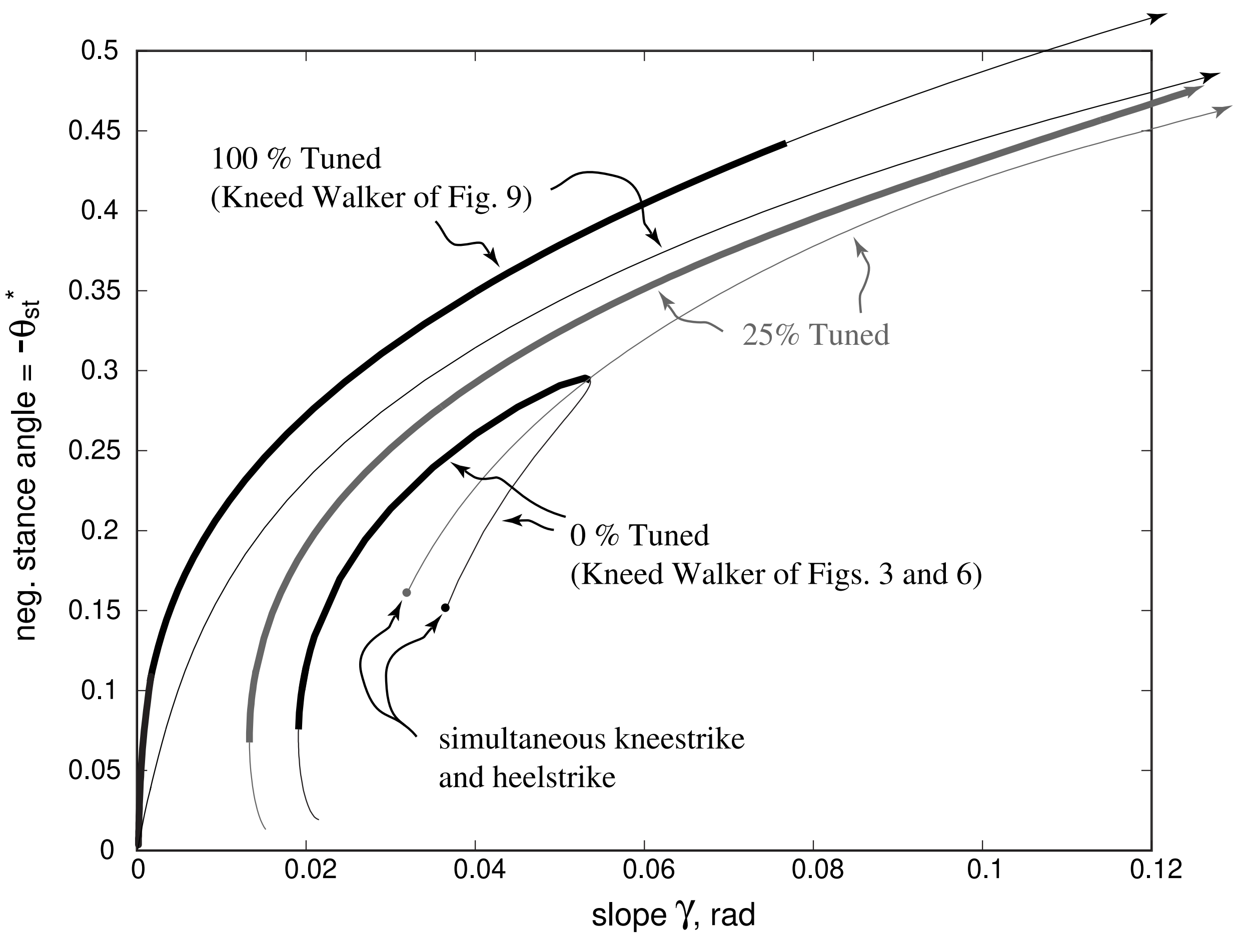

Figure 8: Solution families for three kneed walkers: tuned walker (C) in table 1 (shown in black), the un-tuned walker of figure 3 and figure 6 (also shown in black), and a walker that is 25% tuned (shown in gray). The tuned walker and the 25% tuned walker have distinct short-step and long-step solutions, but as the walker is de-tuned further, the long- and short-step solutions will merge in the upper right portion of the figure and the curve will bend sharply backwards. No solutions were found above the merge point for the 0% tuned walker. That the 25% tuned solution approximately crosses the 0% tuned solution at a stability transition is coincidental.

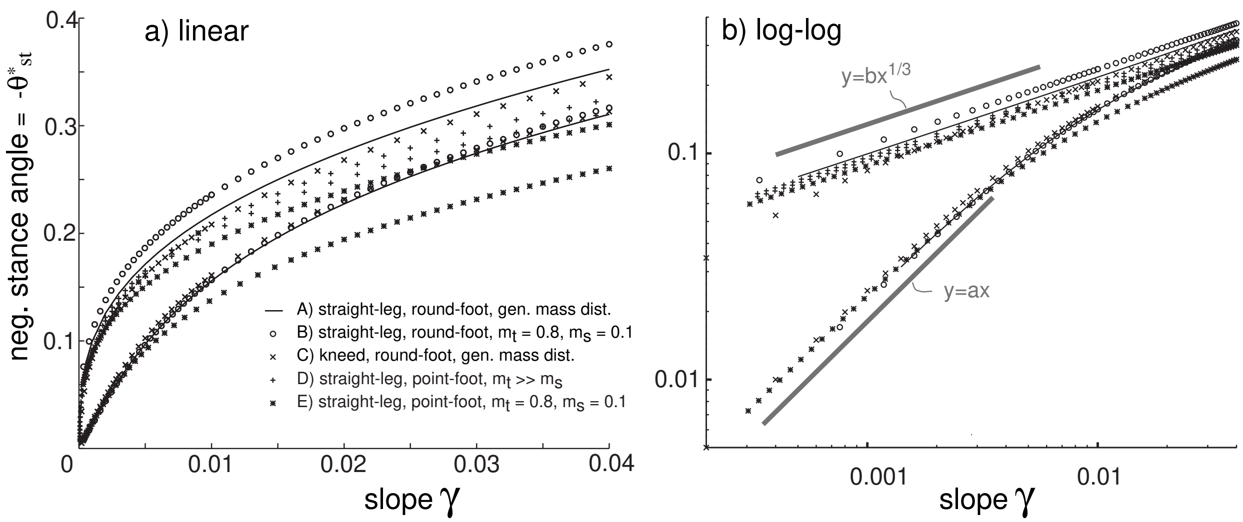

Figure 9: Gait families for tuned zero-slope-capable walkers on (a) a linear plot, and and (b) a log-log plot. Parameter values are listed in table 1. By "gen. mass. dist." it is meant that the parameters are close to those of the kneed walker of figure 3. Note (1) there are two gaits cycles at each γ for all walkers shown; (2) for the "simplest" walker (D) both step lengths are proportional to $\gamma^{1/3}$; (3) the short-step gaits of the other walkers have step lengths proportional to γ for small γ; (4) the long-step gaits for the other walkers have step lengths that are much longer than for the short-step gaits, though not necessarily exactly proportional to $\gamma^{1/3}$ for small γ; and (5) for a point-foot, straight-legged walker with non-negligible foot mass, the step length of the long-step gait *is* proportional to $\gamma^{1/3}$ for small γ.

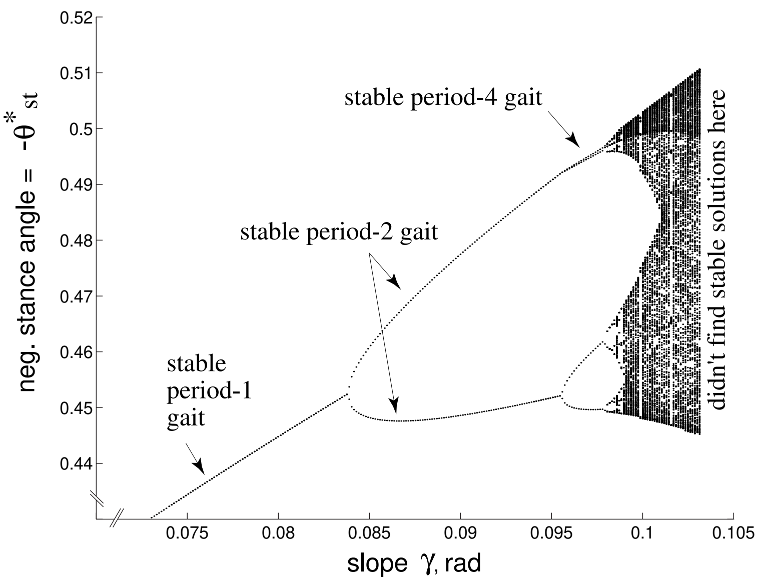

Figure 10: Period doubling of stable kneed walking motions. Only stable walking motions are shown, although all periodic gaits persist as unstable gait cycles after they undergo period-doubling. The parameters are those of the tuned kneed walker (C) in table 1.